Time-Optimal Point-To-Point Motion Planning and Assembly Mode Change of Cuspidal Manipulators: Application to 3R and 6R Robots

Tobias Marauli, Durgesh Haribhau Salunkhe, Hubert Gattringer, Andreas Müller, Damien Chablat, Philippe Wenger

Time-Optimal Point-To-Point Motion Planning and Assembly Mode Change of Cuspidal Manipulators

Tobias Marauli[1] and Durgesh Haribhau Salunkhe[2] and Hubert Gattringer[1] and Andreas Müller[1] and Damien Chablat[2] and Philippe Wenger[2]

***Abstract*— The kinematics of cuspidal 3R regional robots was studied extensively in the past. Moreover, certain industrial 6R robots were found to be cuspidal (e.g. Fanuc CRX series, Kinova GEN2), which makes cuspidal robots finally interesting for practical applications. This necessitates optimal trajectory planning, respecting the dynamics and technical limits of the particular robot. In this paper, a method for singularity-free time-optimal point-to-point trajectory (PtP) trajectory planning is proposed. As a special case, this method is applicable to time-optimal singularity-free assembly mode changing. Results are shown for 3R robots and a 6R Fanuc CRX10iA/L.**

***Index Terms*— Optimization and Optimal Control, Kinematics, Mechanism Design**

I. Introduction

Motivation: The ability to change the assembly mode (i.e. perform a motion that starts and ends with the same end-effector (EE) pose but with different inverse kinematic solution) without having to pass through a singularity is referred to as *singularity-free assembly mode change*. Robots having this ability are called *cuspidal*. Cuspidal robots thus possess at least one singularity free connected region in joint-space, called *c-sheets* [1] or *aspects* [2], with multiple inverse kinematics solutions (IKS). This was first reported in [3], [4]. Historically, the term *cuspidal* stems from the fact that a projection of the critical values (the forward kinematics map of the singularities) exhibits cusps, which is a sufficient condition for 3R manipulators to be cuspidal. This has triggered extensive research on cuspidal 3R serial manipulators [5], [6], [7]. It was recently shown [8] that for generic 3R robots the existence of cusps in workspace is sufficient and necessary to be cuspidal. Research on robot geometries satisfying the necessary cuspidality property was originally pursued for 3R regional robots [5], [9]. A review to the research in cuspidal robots is given by [10], including also parallel mechanisms. Lately it was recognized that also 6R industrial robots are cuspidal, e.g. *Fanuc CRX* series and *Kinova Jaco gen2*, which increases the significance of cuspidality for practical applications. Consequently, to fully exploit this feature, cuspidality should be included in the motion planning process. Optimal trajectory planning based on a dynamic robot model has not yet been addressed for cuspidal robots. Moreover, cuspidality not only allows for singularity-free assembly mode change, it is also enables planning singularity-free point-to-point (PtP) motions. In the following, a example which further highlights the benefits of considering cuspidality in the motion planning process is discussed.

In the course of this paper n-DOF robotic manipulators with only revolute joints are considered. Denote with $\mathbf{q}(t) \in \mathbb{T}^n$ the joint coordinate vector, and with $\mathbf{z} \in W$ the end-effector pose, where $W \subseteq SE(3)$ is the workspace. Further denote with $\mathbf{z} = \mathbf{f}(\mathbf{q})$ the forward kinematics map, and with $\mathbf{J}$ the forward kinematics Jacobian. Kinematic singularities are defined by the hyper-surface $\det \mathbf{J}(\mathbf{q}) = 0$, which divides the joint-space into aspects.

For a conventional (non-cuspidal) wrist-partitioned robot, all IKS for a given EE pose $\mathbf{z}$ belong to one aspect, and are generally referred to as *postures*. For example, the elbow up and elbow down configurations are the two postures of a 2R robot. Similarly, wrist-partitioned robots possess 8 postures. The important point is that each IKS belongs exactly one aspect, and that the robot must pass through a singularity to change posture. Cuspidal robots, on the other hand, have multiple IKS in one aspect. Fig. 1 shows this for a 3R robot with DH parameters $\{a_1, a_2, a_3\} = \{0.5, 1, 0.75\}$m, $\{d_1, d_2, d_3\} = \{0, 0.5, 0\}$m, $\{\alpha_1, \alpha_2, \alpha_3\} = \{-\pi/2, \pi/2, 0\}$. The singularity loci, separating the aspects, are shown as solid lines in joint and task space. For the EE pose $\mathbf{z}_\mathrm{a}$ there are four IKS, denoted with $\mathbf{q}_{\mathrm{a},1}, \dots \mathbf{q}_{\mathrm{a},4}$, and for $\mathbf{z}_\mathrm{b}$ there are two IKS, denoted with $\mathbf{q}_{\mathrm{b},1}, \mathbf{q}_{\mathrm{b},2}$. Importantly, an aspect contains different IKS. This allows to transit from one IKS to another without leaving an aspect, i.e. not crossing a singualrity. The 3R robot can move from $\mathbf{q}_{\mathrm{a},1}$ to $\mathbf{q}_{\mathrm{b},1}$ corresponding to EE pose $\mathbf{z}_\mathrm{a}$ and $\mathbf{z}_\mathrm{b}$, respectively. If the EE has to return to the inital $\mathbf{z}_\mathrm{a}$ (e.g. in a pick and place scenario), it could go to the IKS $\mathbf{q}_{\mathrm{a},2}$. This leads to a non-singular assembly mode change. Another motivation is that in this way collisions can be avoided with obstacles that were not present during the forward motion. Also from a control perspective, it may be more efficient or faster to move from $\mathbf{q}_{\mathrm{b},1}$ to $\mathbf{q}_{\mathrm{a},2}$ instead to $\mathbf{q}_{\mathrm{a},1}$. Such a time optimal trajectory planning and assembly mode change is addressed in this paper.

Contribution: An algorithm for time-optimal point-to-point (PtP) trajectory planning in workspace is proposed in Sec. II, and for time-optimal assembly mode change in Sec. III, which is the special case where initial and terminal EE-pose are identical. The approach solves the combinatorial problem of identifying that pair of IKS corresponding to

*This work was not supported by any organization

[1]Institute of Robotics, Johannes Kepler University Linz, Altenberger Str. 69, 4040 Linz, Austria {tobias.marauli, hubert.gattringer, a.mueller}@jku.at

[2]LS2N, CNRS, F-44321 Nantes, France {durgesh.salunkhe, Damien.Chablat, Philippe.Wenger}@ls2n.fr

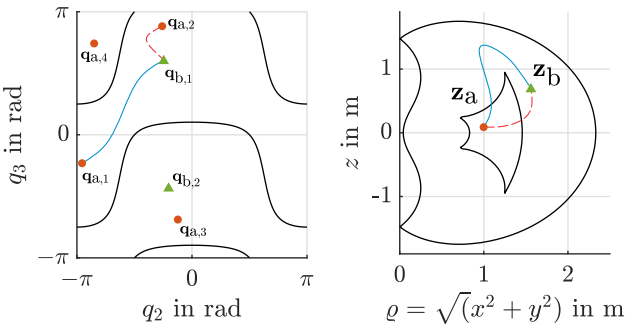

(a) path in joint space (b) PTP path in workspace

Fig. 1: Joint space a) and spherical cut of the workspace b) of a cuspidal 3R robot.

the prescribed initial and terminal EE-pose which admits the fastest trajectory connecting them, while taking all technical limits of the robot into account. To this end, a set of pairs of candidate IKS is determined, and for each pair, a time-optimal trajectory planning problem is solved using a multiple shooting algorithm. The results when applying the method to a 3R robot (only EE positions are used) and a 6R industrial robot are shown in the course of this paper. To the best authors' knowledge, this is the first paper addressing singularity-free time-optimal trajectory planning and assembly mode change of cuspidal robots. In addition to the time-optimal motion, the algorithm enables checking whether singularity-free motions are actually feasible given the joint limits of real robots. The latter has never been taken into account when discussing cuspidal robots.

II. Optimal Non-Singular Trajectory Planning

A. Problem Statement

A major benefit of serial cuspidal manipulators is the presence of regions in work space with more than two IKS that are connected by singularity-free curves in joint space. Denote with

$$\mathcal{I}_{\mathbf{z}} = \{\mathbf{q} \in \mathbb{T}^n \,|\, \mathbf{z} = \mathbf{f}(\mathbf{q})\} \tag{1}$$

the set of IKS for given EE-pose $\mathbf{z}$, which can be computed using e.g. the HUPF-algorithm [11], the approach presented in [8] or roboter specific such as [12] for the Kinova Jaco robot. For a non-redundant robot, i.e. $\dim W = \dim \operatorname{im} f \leq n$, the IKS set consist of a finite $n_{\mathbf{z}}$ number of IKS $\mathcal{I}_{\mathbf{z}} = \{\mathbf{q}_1, \ldots, \mathbf{q}_{n_{\mathbf{z}}}\}$. A necessary condition for two solutions to belong to the same aspect is that the determinant of the Jacobian has the same sign. This is not sufficient, however, since the sign may change multiple times along the trajectory. The set of candidate IKS for an initial solution $\mathbf{q}_0$ and EE-pose $\mathbf{z}$ is introduced as

$$\mathcal{R}_{\mathbf{q}_0,\mathbf{z}} := \{\mathbf{q} \in \mathcal{I}_{\mathbf{z}} \,|\, \operatorname{sign}(\det \mathbf{J}(\mathbf{q}_0)) = \operatorname{sign}(\det \mathbf{J}(\mathbf{q}))\}. \tag{2}$$

Furthermore, the set of pairs of candidate IKS for a given initial EE-pose $\mathbf{z}_0$ and EE-pose $\mathbf{z}$ is introduced as

$$\begin{aligned}\mathcal{R}_{\mathbf{z}_0,\mathbf{z}} := \{&(\mathbf{q}_0, \mathbf{q}) \in \mathcal{I}_{\mathbf{z}_0} \times \mathcal{I}_{\mathbf{z}} \mid \\ &\operatorname{sign}(\det \mathbf{J}(\mathbf{q}_0)) = \operatorname{sign}(\det \mathbf{J}(\mathbf{q}))\} \\ = \{&(\mathbf{q}_0, \mathbf{q}) \in \mathcal{R}_{\mathbf{q},\mathbf{z}_0} \times \mathcal{I}_{\mathbf{z}}\} \\ = \{&(\mathbf{q}_0, \mathbf{q}) \in \mathcal{I}_{\mathbf{z}_0} \times \mathcal{R}_{\mathbf{q}_0,\mathbf{z}}\}.\end{aligned} \tag{3}$$

Problem 1 (Time-Optimal Non-Singular PTP Trajectory Planning in Task Space): Given initial and terminal EE-pose, $\mathbf{z}_0$ and $\mathbf{z}_T$. For all potentially valid IKS combinations $(\mathbf{q}_0, \mathbf{q}_T) \in \mathcal{R}_{\mathbf{z}_0,\mathbf{z}_T}$, find the optimal $(\mathbf{q}_0^*, \mathbf{q}_T^*)$ that allows for the fastest trajectory $\mathbf{q}^*(t)$, with $\mathbf{q}^*(0) = \mathbf{q}_0^*$, $\mathbf{q}^*(T) = \mathbf{q}_T^*$, satisfying all kinematic and dynamic constraints of the robot.

B. Computational Algorithm

The time-optimal non-singular trajectory planning problem in workspace is to determine the optimal pair of candidate IKS that leads to the time-optimal non-singular trajectory between $\mathbf{z}_0$ and $\mathbf{z}_T$. This corresponds to the problem of finding an optimal index $i \in \mathcal{N} = \{1, 2, \ldots, n(\mathcal{R}_{\mathbf{z}_0,\mathbf{z}})\}$, which lead to the the optimal pair $(\mathbf{q}_0, \mathbf{q}_T)^* = (\mathbf{q}_0, \mathbf{q}_T)_{i^*}$ with the minimal duration time T^* between the two EE-poses. This can be written as

$$i^* = \arg\min_{i \in \mathcal{N}} \{T_1, T_2, \ldots\}, \tag{4}$$

where $T_i = T \circ (\mathbf{q}_0, \mathbf{q}_T)_i$ denotes the duration time of a time-optimal trajectory $\mathbf{q}^*(t)$ connecting $\mathbf{q}_{0,i}$ and $\mathbf{q}_{T,i}$. To this end, a time-optimal PtP control problem (OCP) is solved $\forall\, (\mathbf{q}_0, \mathbf{q}_T) \in \mathcal{R}_{\mathbf{z}_0,\mathbf{z}_T}$, to provide to the input data to (4).

1) Time-Optimal Trajectory Planning: For each candidate pair $(\mathbf{q}_0, \mathbf{q}_T) \in \mathcal{R}_{\mathbf{z}_0,\mathbf{z}_T}$, a time-OCP is solved that ensures singularity-free motion. The robot dynamics is represented by the equations of motion (EOM)

$$\mathbf{M}(\mathbf{q})\ddot{\mathbf{q}} + \mathbf{h}(\mathbf{q}, \dot{\mathbf{q}}) = \boldsymbol{\tau} \tag{5}$$

where $\mathbf{M}(\mathbf{q})$ is the mass matrix and $\boldsymbol{\tau}$ are the joint torques. The Coriolis, centrifugal and gravitational terms as well as the Coulomb and viscous friction are described by $\mathbf{h}(\mathbf{q}, \dot{\mathbf{q}})$.

Planing non-singular trajectories requires a measure of distance to the singularity. To this end, the kinematic manipulability $\mu = \sqrt{\det \mathbf{J}\mathbf{W}\mathbf{J}^T}$ (where $\mathbf{W}$ is a scaling matrix) is used [13]. While for 3R serial robots this is well-defined, appropriate scaling is necessary for spatial robots to account for disparate units of EE twists [14]. Denote with ε a threshold on the 'distance' to singularity. The condition on $\mathbf{q}(t)$ being a singularity-free trajectory is

$$\mu(\mathbf{q}(t)) \geq \varepsilon, \quad \operatorname{sign}(\det \mathbf{J}(\mathbf{q}_0)) = \operatorname{sign}(\det \mathbf{J}(\mathbf{q}(t))). \tag{6}$$

The OCP is to find a joint trajectory connecting the IKS $\mathbf{q}_0$ and $\mathbf{q}_T$ in minimum time, while satisfying the physical limits of the robot and ensuring smooth joint trajectories. In most applications it is sufficient to ensure continuous accelerations $\ddot{\mathbf{q}}$. A common strategy to this end is to use the so-called flat system representation [15], [16]. Then the joint jerk $\dddot{\mathbf{q}}$ is used as control input, and the non-linear system dynamics

(5) serves as dynamic constraint. The integrator chain is described as ODE represented by $\dot{\mathbf{x}} = \mathbf{f}(\mathbf{x}, \mathbf{u})$, with state $\mathbf{x}^T = \left[\mathbf{q}^T, \dot{\mathbf{q}}^T, \ddot{\mathbf{q}}^T\right]$ and input $\mathbf{u} = \dddot{\mathbf{q}}$. The objective is a combination of terminal time T and a regularization term for smooth joint jerk [17]. The OCP is then written as a non-linear optimization problem

$$\begin{aligned} \min_{T,\mathbf{x},\mathbf{u}} \; & \left(T + k_j \int_0^T \mathbf{u}^T \mathbf{u} \, \mathrm{d}t \right), \\ \text{s.t.} \;\; & \dot{\mathbf{x}} = \mathbf{f}(\mathbf{x}, \mathbf{u}), \\ & \mathbf{x}(0) = \mathbf{x}_0, \qquad \mathbf{x}(t_\mathrm{T}) = \mathbf{x}_\mathrm{T}, \\ & \underline{\mathbf{x}} \leq \mathbf{x}(t) \leq \overline{\mathbf{x}}, \quad \underline{\mathbf{u}} \leq \mathbf{u}(t) \leq \overline{\mathbf{u}}, \\ & \underline{\boldsymbol{\tau}} \leq \boldsymbol{\tau}(t) \leq \overline{\boldsymbol{\tau}}, \;\; \text{conditions (6)} \\ & \text{for } t \in [0, t_\mathrm{T}], \end{aligned} \tag{7}$$

with $\mathbf{x}_0^T = \left[\mathbf{q}_0^T, \mathbf{0}, \mathbf{0}\right]$ and $\mathbf{x}_T^T = \left[\mathbf{q}_T^T, \mathbf{0}, \mathbf{0}\right]$ as initial and terminal state. The limits on the joint coordinates, velocities, accelerations, jerks, and generalized torques (5) are expressed with the lower and upper bounds denoted with $\underline{()}$, $\overline{()}$. The parameter k_j defines the trade-off between time-optimal and smooth joint jerk trajectories. Non-singular trajectories are ensured by the constraints (6). The OCP is solved with a multiple shooting approach [18] implemented in MATLAB using CasADi [19] and Ipopt [20] as solver.

2) Selection of the Optimal Pair of IKS: The OCP (7) is solved for all candidate pairs $(\mathbf{q}_0, \mathbf{q}_T) \in \mathcal{R}_{\mathbf{z}_0,\mathbf{z}_T}$, and the fastest solution is selected. The time-optimal solution is assumed to be isotropic, i.e. $\mathcal{R}_{\mathbf{z}_0,\mathbf{z}_T}$ is regarded as non-ordered set. That is, if $(\mathbf{q}_0, \mathbf{q}_T)$ has been treated, the pair $(\mathbf{q}_T, \mathbf{q}_0)$ obtained by swapping initial and terminal configuration is not considered. This leads to the Algorithm 1.

Algorithm 1 Time optimal non-singular trajectory planning

Require: EE-pose $\mathbf{z}_0$ and $\mathbf{z}_T \Rightarrow$ IKS $(\mathbf{q}_0, \mathbf{q}_T) \in \mathcal{R}_{\mathbf{z}_0,\mathbf{z}_T}$
  for all $(\mathbf{q}_0, \mathbf{q}_T) \in \mathcal{R}_{\mathbf{z}_0,\mathbf{z}_T}$ **do**
    Solve OCP (7) $\Rightarrow \mathbf{q}_i^*(t)$, T_i
  end for
  With (4), $i^* \Rightarrow (\mathbf{q}_0, \mathbf{q}_T)^*$ and fastest trajectory $\mathbf{q}^*(t)$

Above algorithm takes care of numerical difficulties encountered by the fact that different revolute joint angles are equal modulo 2π. Since these joints can rotate freely within their technological limits, clockwise as well as counter clockwise rotations must be taken into account. The joint coordinates are defined by a n-torus $\mathbb{T}^n$. Therefore, adding $\pm 2k\pi$ with $k \in \mathbb{N}_0$ does not change the IKS i.e. $\mathbf{z} = \mathbf{f}(\mathbf{q}) = \mathbf{f}(\mathbf{q} \pm 2k\pi)$. For practical applications only solutions within the interval $\mathbf{q} \in [-2\pi, 2\pi]$ have to be considered. As example consider planning singularity-free trajectories for a 3R serial manipulator (DH parameters in Sec. I) connecting the IKS in one aspect, as shown in Fig. 2a. A non-singular trajectory between $\mathbf{q}_1$ and $\mathbf{q}_2$ is readily found. On the other hand, planning a trajectory between $\mathbf{q}_3$ and $\mathbf{q}_4$ without crossing a singularity is not possible, since the OCP (7) does not consider the periodicity of the joint coordinates. Therefore, adding $\pm 2\pi$ element-wise to the solution $\mathbf{q}_4$ is extended to the interval $[-2\pi, 2\pi]$ as shown in Fig. 2b. Thus, the IKS $\mathbf{q}_3$ and $\mathbf{q}_4$ can be connected by a non-singular trajectory, with a counter clockwise rotation of the third joint.

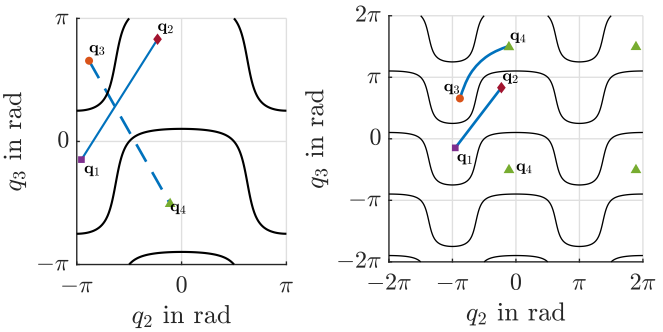

(a) singular connection between IKS $\mathbf{q}_3$ and $\mathbf{q}_4$

(b) singularity-free connection between IKS $\mathbf{q}_3$ and $\mathbf{q}_4$

Fig. 2: Example for considering clockwise and counter clockwise rotations in the IKS.

C. Examples

1) Non-orthogonal serial 3R: Consider a non-orthogonal 3R manipulator with DH parameters $\{a_1, a_2, a_3\} = \{1.178, 0.339, 1\}$m, $\{d_1, d_2, d_3\} = \{0, 0.32, 0.67\}$m, $\{\alpha_1, \alpha_2, \alpha_3\} = \{0, 1.55, -1.124\}$rad [21]. This synthetic robot model was chosen because the aspects are more complicated and consist of singularity encapsulated regions, as can be seen in Fig. 3a. Since no dynamic parameters and physical limits are available for this robot, the dynamic parameters and limits of the *UR10* (first three links) are used to compute physically consistent results. The threshhold of the kinematic manipulability is chosen as $\varepsilon = 10^{-3}$. Exemplary a singularity-free time optimal trajectory between an EE-pose $\mathbf{z}_\mathrm{a}$ in a 4-IKS region and $\mathbf{z}_\mathrm{b}$ in a 2-IKS region, as shown in Fig. 3b, is planned. The corresponding IKS $\mathbf{q}_\mathrm{a} \in \mathcal{I}_{\mathbf{z}_a}$ and $\mathbf{q}_\mathrm{b} \in \mathcal{I}_{\mathbf{z}_b}$ are illustrated in Fig. 3a. Solving the time-optimal non-singular trajectory planning problem (4) with Algorithm 1 leads to the optimal pair $(\mathbf{q}_0, \mathbf{q}_T)^* = (\mathbf{q}_{\mathrm{a},1}, \mathbf{q}_{\mathrm{b},1})$ and the fastest singularity-free time-optimal trajectory $\mathbf{q}^*(t)$, dashed line in Fig.3. It is worth noting, that all combinations including $\mathbf{q}_{\mathrm{a},2}$ lead to an infeasible OCP (7) because the constraint (6) can not be satisfied. This is due to the fact that, $\mathbf{q}_{\mathrm{a},2}$ is within an encapsulated region and therefore no singularity-free trajectory exists. Since, the joint jerk $\dddot{\mathbf{q}}$ is used as control input in the OCP (7) and the torques $\boldsymbol{\tau}$ are the optimal feed-forward, their corresponding trajectories are shown in Fig. 4. Typical for time optimal-solutions at least one constraint is active. By viewing the trajectory $\dddot{q}_3$ the latter is true for nearly the whole trajectory. At the time steps, where $\dddot{q}_3$ is not limited, a joint velocity or acceleration is limited by the constraints. Since the singularities are independent of q_1, the trajectory of the first joint is not restricted as much, which results in lower joint jerks in

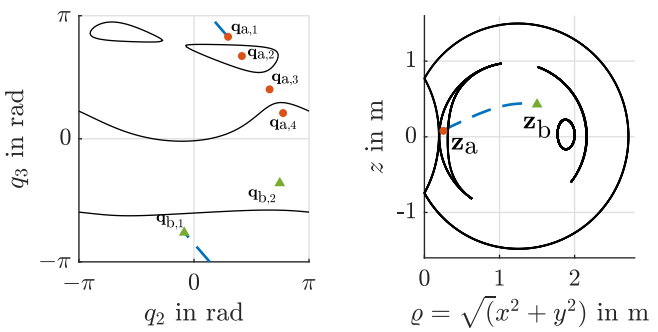

(a) joint-space (b) work-space

Fig. 3: Optimal IKS combination and fastest singularity-free time optimal-trajectory between $\mathbf{z}_\mathrm{a}$ and $\mathbf{z}_\mathrm{b}$ for the non-orthogonal 3R manipulator.

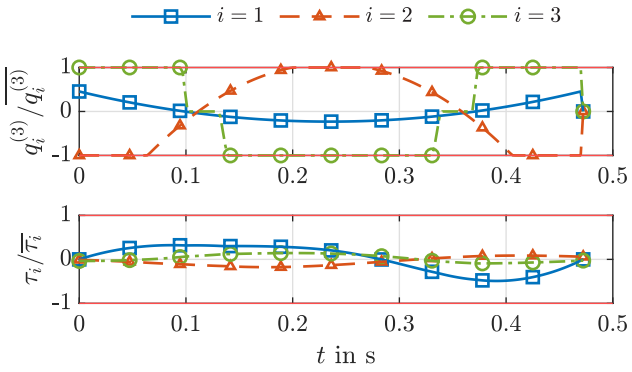

Fig. 4: Normalized joint jerk $\dddot{\mathbf{q}} = \mathbf{q}^{(3)}$ and motor torques $\boldsymbol{\tau}$ of the 3R manipulator traversing from $\mathbf{z}_\mathrm{a}$ to $\mathbf{z}_\mathrm{b}$.

this case. Further, the resulting motor torques are smooth trajectories due to requiring smooth acceleration trajectories.

2) Serial 6R: For the serial 6R cuspidal manipulator the collaborative robot *Fanuc CRX10iA/L* shown in Fig. 5a is chosen, since it is known to be cuspidal. Visualizing the joint and workspace similar to the 3R cuspidal robots becomes quite challenging, since the singularities $\det J(\mathbf{q}) = g(q_2, q_3, q_4, q_5)$ depend on four coordinates and the workspace has 6-DOF. Therefore, a slice of the workspace with fixed orientation and y-coordinate is exemplary shown in Fig. 5b. Again, the optimal pair of IKS which lead to the time-optimal trajectory between an EE-pose $\mathbf{z}_\mathrm{a}$, in a 12-IKS region, and $\mathbf{z}_\mathrm{b}$, in a 8-IKS region has to be found. The joint limits of the Fanuc, are taken from the datasheet available on the Fanuc website. Since, the dynamic parameters of the robot are not known and the Fanuc roughly shares a similar structure to the UR10 the dynamic parameters of the UR10 are used again. The resulting fastest time-optimal non-singular trajectory connecting $\mathbf{z}_\mathrm{a}$ and $\mathbf{z}_\mathrm{b}$ is shown in Fig. 6 as sequence of configurations. The optimal joint jerk $\dddot{\mathbf{q}}$ and torque $\boldsymbol{\tau}$ trajectories are shown in Fig. 11. In this case, different joint limits are limited by their corresponding constraints. Due to lack of space these plots

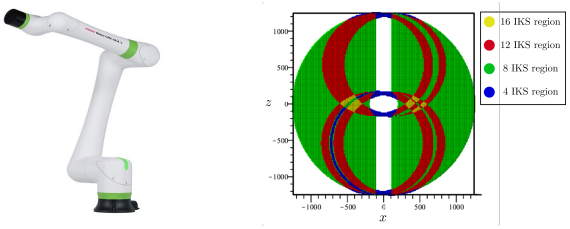

(a) Fanuc CRX 10iA/L (b) Slice of the workspace

Fig. 5: Fanuc CRX 10iA/L and a slice of its workspace for $y = 0.05\,\mathrm{m}$ and orientation represented as Tait-Bryan angles $\alpha_\mathrm{o} = 0.153°$, $\beta_\mathrm{o} = 0.639°$, $\gamma_\mathrm{o} = 0°$.

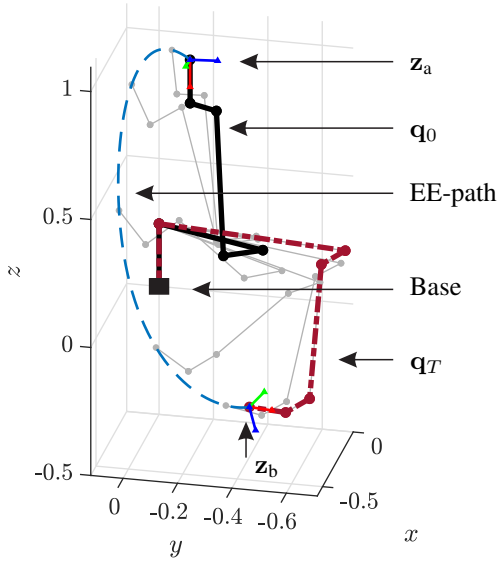

Fig. 6: Optimal IKS combination and fastest non-singular trajectory between $\mathbf{z}_\mathrm{a}$ and $\mathbf{z}_\mathrm{b}$ for the Fanuc CRX10iA/L represented by the kinematic line model.

can not be shown.

III. Optimal Singularity-Free Assembly Mode Change

A. Problem Statement

Changing the IKS solution without crossing singularity is a key feature of cuspidal robots. The problem of finding the corresponding path, connecting two IKS in one aspect without crossing a singularity is referred to as the *connectivity problem*. The latter problem can be defined in various ways. Since this paper focuses on planning time-optimal trajectories the latter problem is defined as time-OCP:

Problem 2 (Time-Optimal Assembly Mode Change Trajectory Planning Problem): Given an IKS $\mathbf{q}_0$ to the EE-pose $\mathbf{z}$. Find $\mathbf{q}_T^*$ of all $\mathbf{q}_T \in \mathcal{R}_{\mathbf{q}_0,\mathbf{z}}$, which yields the fastest trajectory $\mathbf{q}^*(t)$, with $\mathbf{q}^*(0) = \mathbf{q}_0$, $\mathbf{q}^*(T) = \mathbf{q}_T^*$, while satisfying all kinematic and dynamic constraints of the robot.

This is a special case of the problem discussed in Sec. II. If the EE-pose $\mathbf{z}_0$ and $\mathbf{z}_T$ coincide i.e. $\mathbf{z}_0 = \mathbf{z}_T = \mathbf{z}$ and the

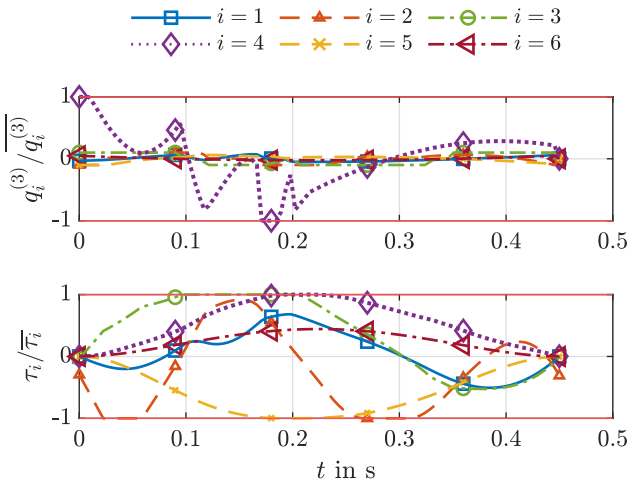

Fig. 7: Normalized joint jerk $\dddot{\mathbf{q}} = \mathbf{q}^{(3)}$ and motor torques $\boldsymbol{\tau}$ of the Fanuc CRX10iA/L traversing from $\mathbf{z}_\mathrm{a}$ to $\mathbf{z}_\mathrm{b}$.

initial IKS $\mathbf{q}_0$ is fixed, Problem 1 degenerated to Problem 2. Therefore, the same algorithm can be used for planning the time-optimal assembly mode change trajectory.

B. Application to Verifying of Cuspidality

Furthermore, solving the time-optimal non-singular assembly mode change problem gives raise to a different approach for checking cuspidality. It is worth noting that the presented approach can terminated without finding a connection between two IKS. Since only one EE-pose $\mathbf{z}$ is checked, this does not imply that the robot is not cuspidal. In order to decide if a robot is cuspidal or not, the connectivity problem has to be solved for the whole workspace until a connection of at least two IKS is found. In [22] a certificated algorithm is presented, which means that the algorithm always checks if a robot is cuspidal or not. The downside of this algorithm is, that it is hard to implement and comes with high computational costs. Therefore, the strategy discussed in this paper can be seen as practical counterpart for checking cuspidality (locally). Moreover, the connectivity problem is solved by considering joint limits in the OCP (7), which are normally not considered for checking cuspidality. Also, collision constraints can be incorporated easily in the verification process by extending the OCP (7) with the latter.

C. Examples

1) Non-orthogonal serial 3R: Consider again the 3R manipulator of Sec. II-C.1. In the following the singularity-free time-optimal assembly mode change trajectory planning problem is solved for the EE-pose $\mathbf{z}_\mathrm{a}$ in a 4 IKS region, as shown in Fig. 8b. In order to show the effect of the threshold value ε on the trajectory planning, the problem is solved for two values $\varepsilon_1 = 10^{-3}$ and $\varepsilon_2 = 30^{-3}$. Choosing $\mathbf{q}_0 = \mathbf{q}_{\mathrm{a},1}$ as desired initial solution, results in the optimal terminal IKS $\mathbf{q}_T^* = \mathbf{q}_{\mathrm{a},3}$. The fastest non-singular time-optimal solution is illustrated in Fig. 8 for either work- and joint-space. Comparing the optimal trajectories of the two ε_1

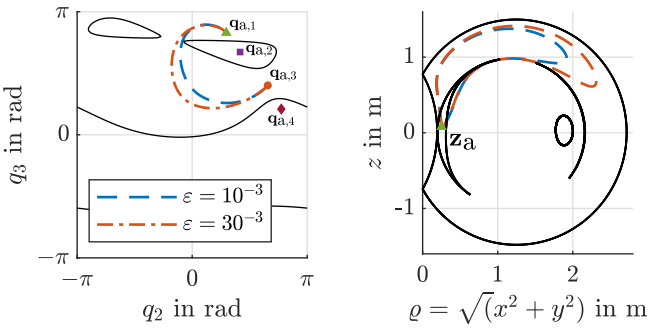

(a) joint-space (b) work-space

Fig. 8: Singularity-free time-optimal assembly mode change of the non-orthogonal 3R manipulator from $\mathbf{q}_{\mathrm{a},1}$ to $\mathbf{q}_{\mathrm{a},3}$.

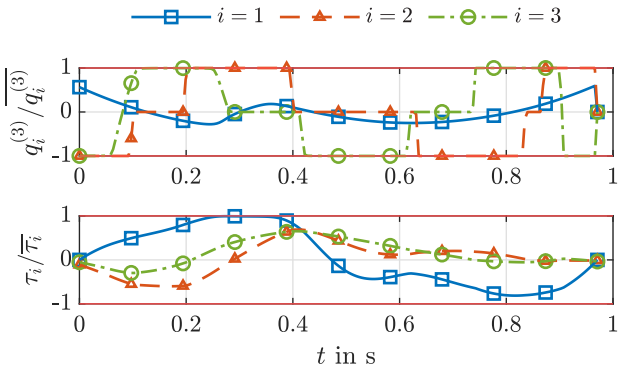

Fig. 9: Normalized joint jerk $\dddot{\mathbf{q}} = \mathbf{q}^{(3)}$ and motor torques $\boldsymbol{\tau}$ of the 3R manipulator performing the non-singular assembly mode change.

and ε_2 a significant difference is already investigated, despite the small increase of ε. The minimal time increases from $T_1 = 0.971\,\mathrm{s}$ to $T_2 = 1.025\,\mathrm{s}$, which is a loss of $5.6\,\%$ in time. It is worth noting that completely different trajectories can be planned, depending on the shape of the aspects and the value of ε. The corresponding control input $\dddot{\mathbf{q}}$ as well as the evolution of the feed-forward i.e. $\boldsymbol{\tau}$ are shown in Fig. 9 for ε_1. As can be seen, the joint jerk constraints are active most of the time.

2) Serial 6R: Finally, the connectivity problem is solved for the Fanuc CRX10iA/L. The non-singular time-optimal assembly mode change is computed for the same EE-pose $\mathbf{z}_\mathrm{b}$ as in Sec. II-C.2, which is in 8-IKS region. The threshhold for the singularity is chosen to be $\varepsilon = 10^{-3}$. The resulting time-optimal singularity-free assembly mode change is shown in Fig. 10 as sequence of configurations. These results, show that the Fanuc CRX10iA/L is even cuspidal, when joint limits are considered. For completeness, the optimal joint jerk $\dddot{\mathbf{q}}$ and torque $\boldsymbol{\tau}$ trajectories are shown in Fig. 11.

IV. Conclusion

A method for time-optimal PtP trajectory planning and assembly mode change was proposed. The method selects the optimal combination among all pairs of admissible candiate

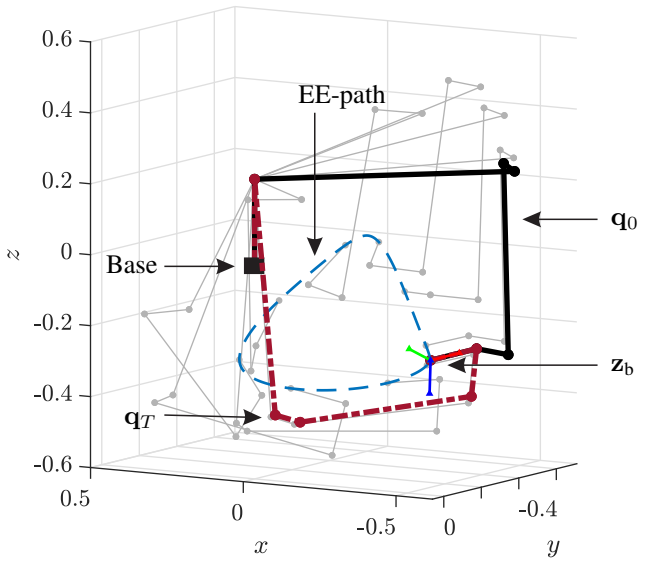

Fig. 10: Time-optimal singularity-free assembly mode change of the Fanuc CRX10iA/L at the EE-pose $\mathbf{z}_b$.

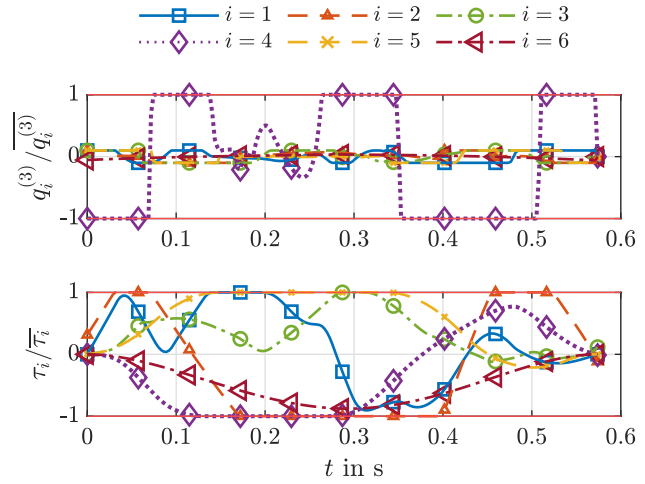

Fig. 11: Normalized joint jerk $\dddot{\mathbf{q}} = \mathbf{q}^{(3)}$ and motor torques $\boldsymbol{\tau}$ of the Fanuc CRX10iA/L performing the non-singular assembly mode change.

IKS. To this end, time-optimal trajectories for all candidate pars are computed with a multiple shooting algorithm. An important issue that is automatically taken into account is to ensure that the non-singular trajectories (which may exist if no restrictions of the joint space is considered) are in fact executable by a real robot given the specific joint limits. Future work will incorporate collision avoidance, including time-dependent obstacles in the trajectory planning. This is when process, to further exploit the advantage of a non-singular IKS change, is of high interest and will be addressed in future work. Moreover, the fact that IKS can vanish when following a path as addressed in [23] is a big issue, since the initial IKS can not be chosen freely. This also impacts the repeatability of closed EE-paths as required for e.g. welding processes, because the initial and terminal EE-pose are not necessarily equal. This briefly explained problems are of high research interest and will be covered also in future work.

References

[1] D. R. Smith, "Design of solvable 6r manipulators," Ph.D. dissertation, Georgia Institute of Technologie, Atlanta, 1990.

[2] P. Borrel and A. Liegeois, "A study of multiple manipulator inverse kinematic solutions with applications to trajectory planning and workspace determination," *Proceedings. 1986 IEEE International Conference on Robotics and Automation*, 1986.

[3] J. W. Burdick, "On the Inverse Kinematics of Redundant Manipulators: Characterization of the Self-Motion Manifolds," in *1989 International Conference on Advanced Robotics*, 1989.

[4] C. Innocenti and V. Parenti-Castelli, "Singularity-free evolution from one configuration to another in serial and fully-parallel manipulators," *ASME J. Mechanical Design*, 1998.

[5] P. Wenger and J. El Omri, "Comments on "A classification of 3R regional manipulator geometries and singularities"," *Mechanism and Machine Theory*, 1997.

[6] P. Wenger, "A New General Formalism for the Kinematic Analysis of All Non-redundant Manipulators," in *Proceedings of the 1992 IEEE International Conference on Robotics and Automation*, Nice, France, 1992.

[7] P. Wenger and D. Chablat, "Robots cuspidaux : théorie et applications," *Les Techniques de l'Ingenieur*, 2021.

[8] D. H. Salunkhe, C. Spartalis, J. Capco, D. Chablat, and P. Wenger, "Necessary and sufficient condition for a generic 3r serial manipulator to be cuspidal," *Mechanism and Machine Theory*, 2022.

[9] P. Wenger, "Classification of 3r positioning manipulators," *Journal of Mechanical Design*, 1998.

[10] P. Wenger and D. Chablat, "A review of cuspidal serial and parallel manipulators," *Journal of Mechanisms and Robotics*, 2023.

[11] M. L. Husty, M. Pfurner, and H.-P. Schröcker, "A new and efficient algorithm for the inverse kinematics of a general serial 6r manipulator," *Mechanism and machine theory*, 2007.

[12] C. Gosselin and H. Liu, "Polynomial inverse kinematic solution of the jaco robot," in *International Design Engineering Technical Conferences and Computers and Information in Engineering Conference*, 2014.

[13] K. L. Doty, C. Melchiorri, E. M. Schwartz, and C. Bonivento, "Robot manipulability," *IEEE Transactions on Robotics and Automation*, 1995.

[14] J. Angeles, "Is there a characteristic length of a rigid-body displacement?" *Mechanism and Machine Theory*, 2006.

[15] H. K. Khalil, "Nonlinear systems third edition," *Patience Hall*, vol. 115, 2002.

[16] E. D. Markus, J. T. Agee, and A. A. Jimoh, "Flat control of industrial robotic manipulators," *Robotics and Autonomous Systems*, 2017.

[17] A. Gasparetto and V. Zanotto, "A technique for time-jerk optimal planning of robot trajectories," *Robotics and Computer-Integrated Manufacturing*, 2008.

[18] H. Bock and K. Plitt, "A multiple shooting algorithm for direct solution of optimal control problems*," *IFAC Proceedings Volumes*, 1984.

[19] J. A. E. Andersson, J. Gillis, G. Horn, J. B. Rawlings, and M. Diehl, "CasADi – A software framework for nonlinear optimization and optimal control," *Mathematical Programming Computation*, 2019.

[20] A. Wächter and L. T. Biegler, "On the implementation of an interior-point filter line-search algorithm for large-scale nonlinear programming," *Mathematical programming*, 2006.

[21] D. Paganelli, "Topological analysis of singularity loci for serial and parallel manipulators," Ph.D. dissertation, Alma Mater Studiorum - Unbersity of Bologna, 2008.

[22] D. Chablat, R. Prébet, M. Safey El Din, D. H. Salunkhe, and P. Wenger, "Deciding cuspidality of manipulators through computer algebra and algorithms in real algebraic geometry," in *Proceedings of the 2022 International Symposium on Symbolic and Algebraic Computation*. Association for Computing Machinery, 2022.

[23] D. H. Salunkhe, D. Chablat, and P. Wenger, "Trajectory planning issues in cuspidal commercial robots," in *Proceedings of the 2023 IEEE International Conference on Robotics and Automation*, London, United Kingdom, 2023.